

Emerging applications of integrated optical micro-combs for analogue RF and microwave photonic signal processing

Xingyuan Xu,¹ Jiayang Wu,¹ Sai T. Chu,³ Brent E. Little,⁴ Roberto Morandotti,⁵
Arnan Mitchell,² and David J. Moss^{1,*}

¹Centre for Micro-Photonics, Swinburne University of Technology, Hawthorn, VIC 3122 Australia

²School of Engineering, RMIT University, Melbourne, VIC 3000, Australia

³Department of Physics and Material Science, City University of Hong Kong, Hong Kong, China.

⁴Xi'an Institute of Optics and Precision Mechanics Precision Mechanics of CAS, Xi'an, China.

⁵INRS – Énergie, Matériaux et Télécommunications, Varennes, Québec, J3X 1S2, Canada.

[*dmoss@swin.edu.au](mailto:dmoss@swin.edu.au)

Abstract

We review new applications of integrated micro-combs in RF and microwave photonic systems. We demonstrate a wide range of powerful functions including a photonic intensity high order and fractional differentiators, optical true time delays, advanced filters, RF channelizer and other functions, based on a Kerr optical comb generated by a compact integrated micro-ring resonator, or “micro-comb”. The micro-comb is CMOS-compatible and contains a large number of comb lines, which can serve as a high-performance multi-wavelength source for the transversal filter, thus greatly reduce the cost, size, and complexity of the system. The operation principle of these functions is theoretically analyzed, and experimental demonstrations are presented.

Keywords: Optical frequency combs, micro-ring resonator, optical signal processing.

1. INTRODUCTION

Nonlinear optics for all-optical signal processing has proven to be an extremely powerful approach, particularly when implemented in photonic integrated circuits based on highly nonlinear materials such as silicon [1, 2]. Functions that have been demonstrated include all-optical logic [3], demultiplexing from 160Gb/s [4] to over 1Tb/s [5], to optical performance monitoring using slow light at speeds of up to 640Gb/s [6-7], all-optical regeneration [8,9], and many others [10-16]. CMOS compatible platforms are centrosymmetric, and so nonlinear devices have been based on a range of third order nonlinear processes including third harmonic generation [11,17-21] and, more commonly, the Kerr nonlinearity (n_2) [1,2]. The efficiency of Kerr based all-optical devices depends on the waveguide nonlinear parameter, $\gamma = \omega n_2 / c A_{\text{eff}}$ where n_2 is the Kerr nonlinearity and A_{eff} is the waveguide effective area). Although silicon can achieve extremely high values of γ , it suffers from high nonlinear losses due to two-photon absorption (TPA) and the resulting free carriers [2]. Even if the free carriers are eliminated by p-i-n junctions, silicon's poor intrinsic nonlinear figure of merit ($\text{FOM} = n_2 / (\beta \lambda)$, where β is the TPA) of around 0.3 in the telecom band is far too low to achieve high performance. While TPA can be turned to advantage for some all-optical functions [22-24], for the most part silicon's low FOM in the telecom band is a limitation. This has motivated research on a range of alternate nonlinear platforms highlighted by perhaps by the chalcogenide glasses[25-35]. While offering many advantages, these platforms however do not offer the compatibility with the silicon computer chip industry – CMOS (complementary metal oxide semiconductor).

In 2008 to 2010, new CMOS compatible platforms for nonlinear optics, including silicon nitride [35,36] and Hydex [37-47] were introduced that exhibit negligible nonlinear absorption in the telecom band, a moderate nonlinear parameter and extremely high nonlinear figure of merit, which are ideal for micro-comb generation [47]. Following the first report of Kerr frequency comb sources in 2007 [48], the first integrated CMOS compatible integrated optical parametric oscillators were reported in 2010 [46, 47], and since then this field has exploded [47]. Many cutting-edge applications have been demonstrated based on CMOS-compatible micro-combs, ranging from filter-driven mode-locked lasers [49-52] to quantum physics [53-58]. Most recently, Kerr micro-combs have demonstrated their enormous potential for sources for ultrahigh bandwidth coherent optical fiber communications[59], optical frequency synthesis [60] and many other applications [61-68]. The success of these new CMOS platforms as well as other CMOS platforms such as amorphous silicon [69] arises from a combination of their low linear loss, moderate to high nonlinearity and low or even negligible nonlinear loss (TPA).

An emerging and very powerful application of micro-ring resonator based Kerr frequency combs - “microcombs” [47] - has been in the area of radio frequency (RF) and microwave photonics that bring together the worlds of radiofrequency engineering and optoelectronics [70-90]. RF and microwave photonics exploit the potential of optical technologies and offers many benefits for RF systems including high speed, broad operation bandwidth, low loss, and strong immunity to electromagnetic interference. A diverse range of photonic approaches to RF signal generation, transmission, processing, and sensing have been proposed and widely employed in RF systems and communication networks[91-117]. However, most RF systems are composed of discrete components, which impose certain drawbacks in terms of cost, power consumption and reliability, thus holding RF photonic systems from reaching maturity and replacing traditional RF solutions. As one of the most powerful tools in RF photonic systems, optical frequency combs offer an alternative as multi-wavelength sources for multiple RF channels, and thus can greatly increase the capacity for transmission and performance for transversal processors. This is particularly true of optical micro-combs [47, 118-129].

Here, we review our recent progress in applications of optical micro-combs to RF and microwave photonics [118]. In particular, we demonstrate a reconfigurable RF photonic intensity differentiator [124] based on CMOS-compatible micro-combs. By employing an on-chip nonlinear micro-ring resonator (MRR), we generate a broadband Kerr comb with a large number of comb lines and use it as a high-quality multi-wavelength source for a transversal differentiator. The large frequency spacing of the integrated Kerr comb yields a potential operation bandwidth of over 100 GHz, well beyond the processing bandwidth of electronic devices. By programming and shaping the power of individual comb lines according to corresponding tap weights, reconfigurable intensity differentiators with variable differentiation orders can be achieved. Detailed analyses of the operation principle and experimental demonstrations of fractional-, first-, second-, and third-order intensity differentiations are performed. We also present results on optical true time delays for radar applications [129], programmable RF filters [122] and other advanced functions [122]. Optical micro-combs offer powerful solutions to implement RF and microwave photonic signal processing functions.

2. OPERATION PRINCIPLES

Based on the theory of signals and systems, the spectral transfer function of an N -th order temporal differentiator can be expressed as

$$H(\omega) \propto (j\omega)^N, \quad (1)$$

where $j = \sqrt{-1}$, ω is the angular frequency, and N is the differentiation order. According to the above transfer function, the amplitude response of a temporal differentiator is proportional to $|\omega|^N$, while the phase response has a linear profile, with a zero and π jump at zero frequency for N even and odd, respectively. The ideal RF amplitude and phase responses of first-, second-, and third-order microwave differentiators are shown in Figs. 1(a)–(c), respectively.

We employ [114] a versatile approach towards the implementation of microwave photonic differentiators based on transversal filters, where a finite set of delayed and weighted replicas of the input RF signal are produced in the optical domain and combined upon detection. The transfer function of a typical transversal filter can be described as

$$H(\omega) = \sum_{n=0}^{M-1} a_n e^{-j\omega nT}, \quad (2)$$

where M is the number of taps, a_n is the tap coefficient of the n^{th} tap, and T is the time delay between adjacent taps. It should be noted that the differentiator designed based on Eq. (2) is an intensity differentiator, i.e., the output RF signal after being combined upon detection yields an exact differentiation of the input RF signal, in contrast to field differentiators that yield the derivative of a complex optical field [92-96]. Figure 1(f) depicts the difference between field differentiation and intensity differentiation.

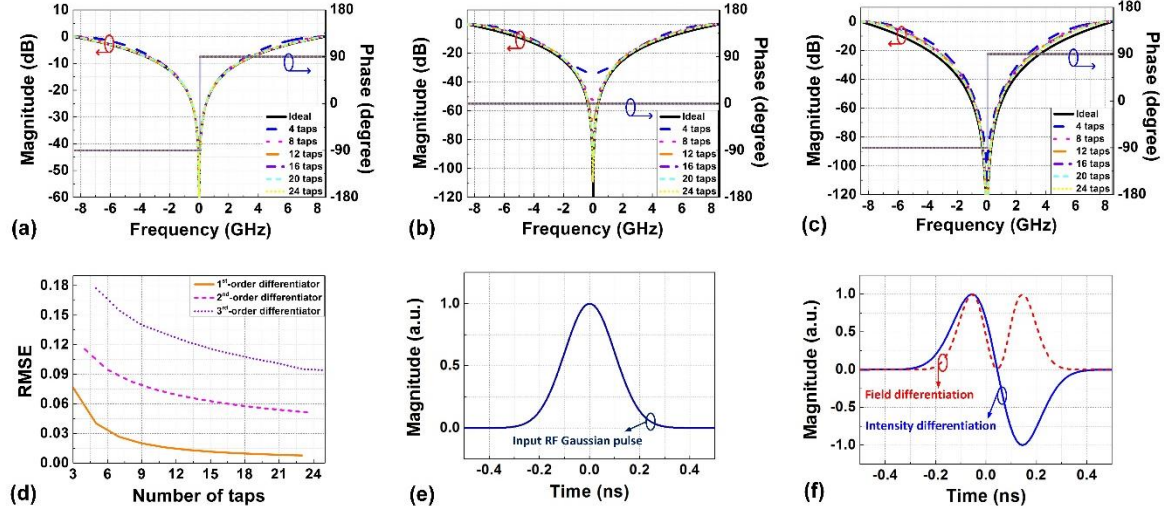


Fig. 1. Simulated RF amplitude and phase responses of the (a) first-, (b) second-, and (c) third-order temporal differentiators. The amplitude and phase responses of the differentiators designed based on Eq. (2) with different number of taps are also shown accordingly. (d) RMSEs between calculated and ideal RF amplitude responses of the first-, second-, and third-order intensity differentiators as a function of the number of taps. Simulated (e) input Gaussian pulse and its corresponding first-order differentiation results.

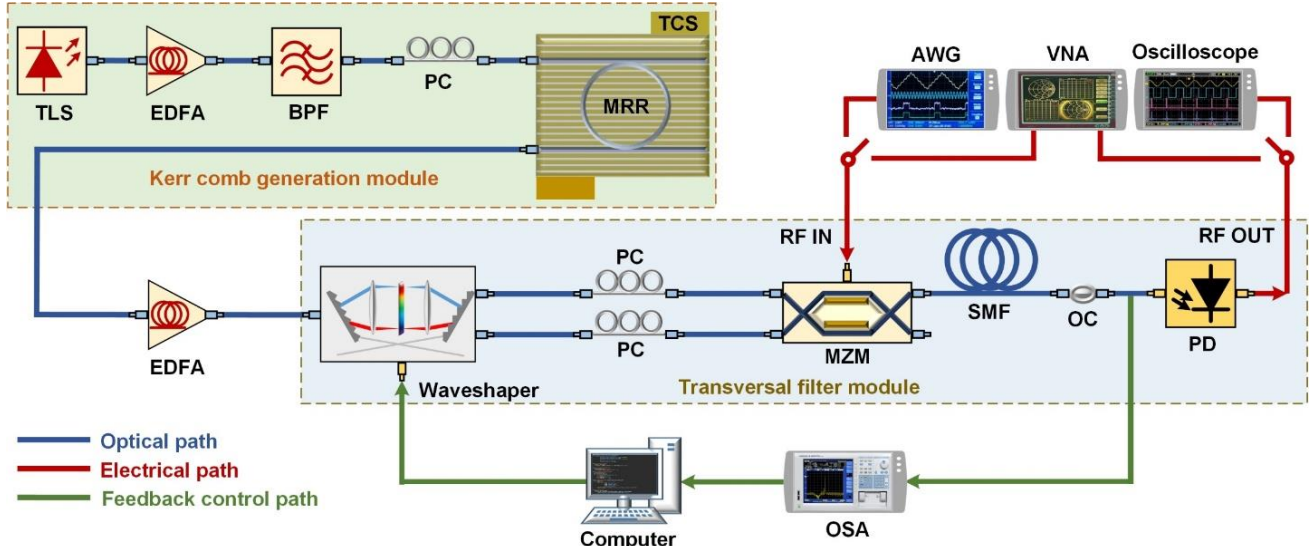


Fig. 2. Schematic illustration of the proposed reconfigurable microwave photonic intensity differentiator. TLS: tunable laser source. EDFA: erbium-doped fibre amplifier. PC: polarization controller. BPF: optical bandpass filter. TCS: temperature control stage. MZM: Mach-Zehnder modulator. SMF: single mode fibre. OC: optical coupler. PD: photo-detector. OSA: optical spectrum analyzer. VNA: vector network analyzer. AWG: arbitrary waveform generator.

To implement the temporal differentiator in Eq. (1), we calculate the tap coefficients in Eq. (2) based on the Remez algorithm [114]. The corresponding amplitude and phase responses of the first-, second-, and third-order differentiators as a function of the numbers of taps are also plot in Figs. 1(a)–(c). When the number of taps is increased, it is clear that the discrepancies between the amplitude response of the transversal filters and the ideal differentiators are improved for all three orders, whereas the phase response of the transversal filters is identical to that of the ideal differentiators regardless of the number of taps. To quantitatively analyze the discrepancies in the amplitude response, we further calculate the root mean square errors (RMSEs) for the first-, second-, and third-order differentiators as a function of the number of taps, as shown in Fig. 1(d). One can see that the RMSE is inversely proportional to the number of taps, as reasonably expected. In

particular, we note that when the number of taps increases, the RMSE decreases dramatically for a small number of taps, and then decreases more gradually as the number of taps becomes larger.

Figure 2 shows a schematic illustration of the reconfigurable microwave photonic intensity differentiator [124]. It consists of two main blocks: one is a Kerr comb generation module based on a nonlinear MRR and the other is a transversal filter module for reconfigurable intensity differentiation. In the first module, the continuous-wave (CW) light from a tunable laser source is amplified by an erbium-doped fibre amplifier (EDFA), followed by a tunable optical bandpass filter to suppress the amplified spontaneous emission noise. A polarization controller is inserted before the nonlinear MRR to make sure that the polarization state matches the desired coupled mode. When the wavelength of the CW light is tuned to a resonance of the nonlinear MRR and the pump power is high enough for sufficient parametric gain, the optical parametric oscillation (OPO) process in the nonlinear MRR is initiated, which generates a Kerr optical comb with nearly equal line spacing. The nonlinear MRR is mounted on a highly precise temperature control stage to avoid resonance drifts and maintain the wavelength alignment of the resonance to the CW light. Owing to the compact size and ultra-high quality factor of the nonlinear MRR, the generated Kerr comb provides a large number of wavelength channels with narrow linewidths for the subsequent transversal filter module. As compared to conventional intensity differentiators based on laser diode arrays, the cost, size and complexity can be greatly reduced. After being amplified by another EDFA, the generated Kerr comb then is directed to the second module. The Kerr comb is processed by a waveshaper to get weighted taps according to the coefficients calculated by means of the Remez algorithm. Considering that the generated Kerr comb is not flat, a real-time feedback control path is introduced to read and shape the comb lines' power accurately. A 2×2 balanced Mach-Zehnder modulator (MZM) is employed to generate replicas of the input RF signal. When the MZM is quadrature-biased, it can simultaneously modulate the input RF signal on both positive and negative slopes, thus yielding modulated signals with opposite phases and tap coefficients with opposite algebraic signs. After being modulated, the tapped signals from one output of the MZM are delayed by a dispersive fibre. The time delay between adjacent taps is determined jointly by the frequency spacing of the employed comb source and the dispersion accumulated in the fibre. Finally, the weighted and delayed taps are combined upon detection and converted back into RF signals to form the differentiation output.

Due to the intrinsic advantages of transversal filters, this scheme features a high degree of reconfigurability in terms of processing functions and operation bandwidth, thus offering a reconfigurable platform for diverse microwave photonic computing functions. By programming the waveshaper to shape the comb lines according to the corresponding tap coefficients, this scheme can also apply to other computing functions such as Hilbert transforms[123]. The operation bandwidth can also be changed by adjusting the time delay between adjacent taps or employing different tap coefficients. An increased operation bandwidth can be achieved by simply employing a dispersive fibre with shorter length. The operation bandwidth is fundamentally limited by the Nyquist zone, which is determined by the comb spacing. In our case, the frequency spacing of the Kerr comb generated by the nonlinear MRR reaches 200 GHz, thus leading to a potential operation bandwidth of over 100 GHz.

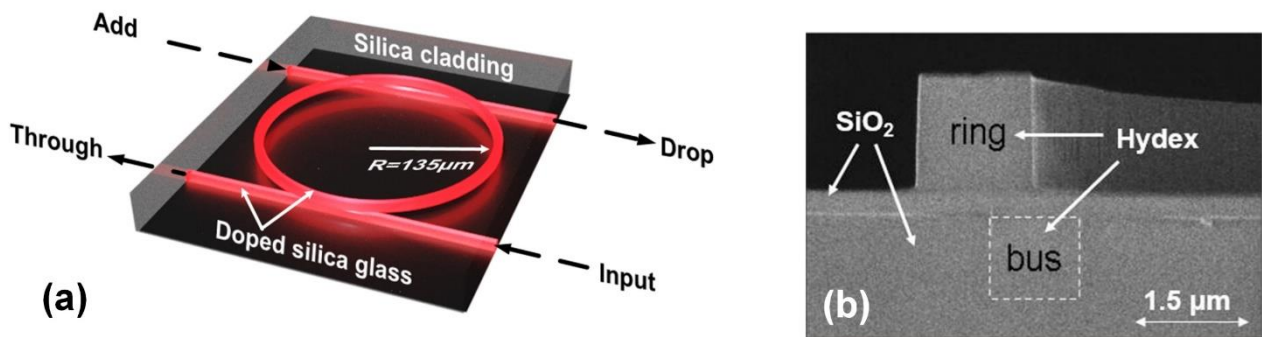


Fig. 3. (a) Schematic illustration of MRR. (b) SEM image of the cross-section of the MRR before depositing the SiO₂ upper cladding.

3. EXPERIMENTAL RESULTS

In our experiment, as Fig. 3(a) shows, the nonlinear MRR used to generate the Kerr comb was fabricated on a high-index doped silica glass platform using CMOS compatible fabrication processes [28]. First, high-index ($n = 1.7$) doped silica glass films were deposited using standard plasma enhanced chemical vapour deposition (PECVD), then photolithography and reactive ion etching (RIE) were employed to form waveguides with exceptionally low surface roughness. Finally, the waveguides were buried in a lower index upper cladding. The radius of the Hydex MRR is $\sim 135 \mu\text{m}$. The compact integrated MRR has a large free spectral range (FSR) of $\sim 1.6 \text{ nm}$, i.e., $\sim 200 \text{ GHz}$. Such a large FSR enables an increased Nyquist zone of $\sim 100 \text{ GHz}$, which is challenging for mode-locked lasers and externally-modulated comb sources. The advantages of the platform for integrated nonlinear optics include ultra-low linear loss ($\sim 0.06 \text{ dB} \cdot \text{cm}^{-1}$), a moderate nonlinearity parameter ($\sim 233 \text{ W}^{-1} \cdot \text{km}^{-1}$), and in particular a negligible nonlinear loss up to extremely high intensities ($\sim 25 \text{ GW} \cdot \text{cm}^{-2}$). After packaging the input and output ports of the device with fibre pigtailed, the total insertion loss is $\sim 3.5 \text{ dB}$. A scanning electron microscope (SEM) image of the cross-section of the MRR before depositing the SiO_2 upper cladding is shown in Fig. 3(b). By boosting the power of the CW light from the TLS via an EDFA and adjusting the polarization state, multiple mode-spaced combs were first generated, in which the primary spacing was determined by the parametric gain. When the parametric gain lobes became broad enough, secondary comb lines with a spacing equal to the FSR of the MRR were generated via either degenerate or non-degenerate four wave mixing (FWM). In our experiment, the power threshold for the generation of secondary comb lines was $\sim 500 \text{ mW}$.

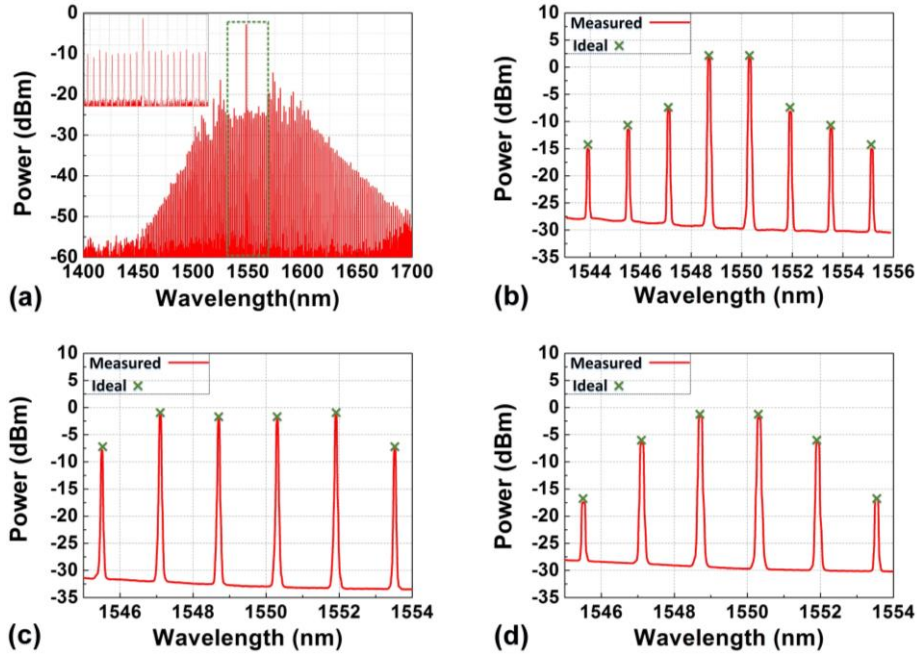


Fig. 4. (a) Optical spectrum of the generated Kerr comb in a 300-nm wavelength range. Inset shows a zoom-in spectrum with a span of $\sim 32 \text{ nm}$. (b)–(d) Measured optical spectra (red solid) of the shaped optical combs and ideal tap weights (green crossing) for the first-, second-, and third-order intensity differentiators.

The resulting Type II Kerr optical comb [37] as shown in Fig. 4(a) is over 200-nm wide, and flat over $\sim 32 \text{ nm}$. Since the generated comb only served as a multi-wavelength source for the subsequent transversal filter in which the optical power from different taps was detected incoherently by the photo-detector, the coherence of the comb was not crucial and the proposed differentiator was able to work under relatively incoherent conditions, although by necessity avoiding the chaotic regime [37]. In the experiment, the numbers of taps used for fractional-, first-, second-, and third-order differentiation demonstrations were 7, 8, 6, and 6, respectively. The choice of these numbers was made mainly by considering the power dynamic range of the comb lines, i.e., the difference between the maximum power of the generated comb lines and the power associated with the noise floor. The power dynamic range was determined by the EDFA before waveshaping, and in our case, it was $\sim 30 \text{ dB}$. An increased number of taps requires a broader power dynamic range, which can be achieved by using an EDFA with a lower noise floor. As analysed in section 2, more taps are needed when the differentiation order increases, and for a fixed number of taps, increasing the order of differentiation also increases the required power dynamic

range. In order to get better performance with a limited number of taps, we decreased the operation bandwidth of the second- and third-order differentiators to half of the transversal filter's Nyquist frequency when designing the response function with the Remez algorithm. It should be noted that the actual bandwidth of the differentiator is not limited by this design since the FSR of the transversal filter can be enlarged. The calculated tap coefficients for fractional-, first-, second-, and third-order differentiations are listed in Table I. The selected comb lines of the generated optical comb were processed by the waveshaper based on these coefficients. Considering that the generated Kerr comb was not flat, we adopted a real-time feedback control path to increase the accuracy of comb shaping. The comb lines' power was first detected by an optical spectrum analyzer (OSA) and compared with the ideal tap weights, and then an error signal was generated and fed back into the waveshaper to calibrate the system and achieve accurate comb processing. The shaped optical combs are shown in Figs. 4(b)–(d). A good match between the measured comb lines' power (red solid line) and the calculated ideal tap weights (green crossing) was achieved, indicating that the comb lines were successfully shaped. They were then divided into two parts according to the algebraic sign of the tap coefficients and fed into the 2×2 balanced MZM biased at quadrature. The modulated signal after the MZM was propagated through ~ 2.122 -km single mode (dispersive) fibre (SMF). The dispersion of the SMF is ~ 17.4 ps/(nm \cdot km), which corresponds to a time delay of ~ 59 ps between adjacent taps and yields an effective FSR of ~ 16.9 GHz in the RF response spectra.

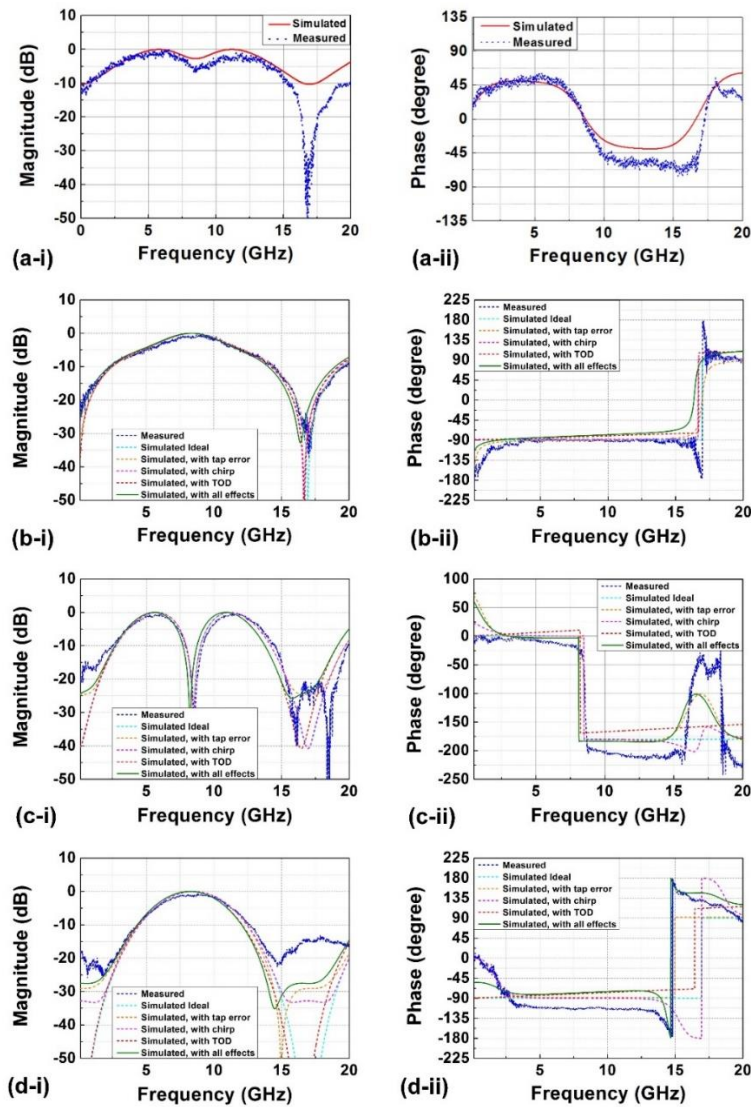


Fig. 5. Measured and simulated RF amplitude and phase responses of (a-i)–(a-ii) the fractional-order, (b-i)–(b-ii) the first-order, (c-i)–(c-ii) second-order, and (d-i)–(d-ii) third-order intensity differentiators. The simulated amplitude and phase responses after incorporating the tap error, chirp, and the third-order dispersion (TOD) are also shown accordingly.

Table 1.

Tap coefficients for the fractional-, first-, second-, and third-order differentiations.

Order of differentiation	Number of taps	Tap coefficients
Fractional-order	7	[0.0578, -0.1567, 0.3834, 1, -0.8288, 0.0985, -0.0892]
First-order	8	[-0.0226, 0.0523, -0.1152, 1, -1, 0.1152, -0.052, 0.0226]
Second-order	6	[0.0241, -0.1107, 0.0881, 0.0881, -0.1107, 0.0241]

After the weighted and delayed taps were combined upon detection, the RF responses for different differentiation orders were characterized by a vector network analyser. Figures. 5(a-i), (b-i), (c-i) and (d-i) show the measured and simulated amplitude frequency responses of the first-, second-, and third-order intensity differentiators, respectively. The corresponding phase responses are depicted in Figs. 5(a-ii), (b-ii), (c-ii) and (d-ii). It can be seen that all three differentiators feature responses close to that expected from ideal differentiations. The FSR of the RF response spectra is ~ 16.9 GHz, which is consistent with the time delay between adjacent taps, as calculated before measurement. Note that by adjusting the FSR of the proposed transversal filter through the dispersive fibre or by programming the tap coefficients, a variable operation bandwidth for the intensity differentiator can be achieved, which is advantageous for meeting diverse requirements in operation bandwidth.

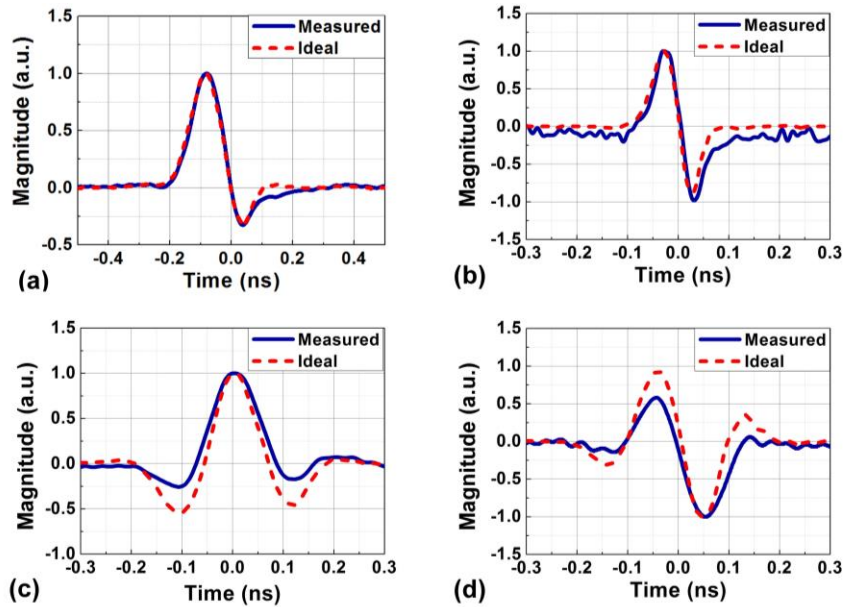


Fig. 6. Theoretical (red dashed) and experimental (blue solid) responses of the (a) fractional- (b) first-, (b) second-, and (c) third-order intensity differentiators.

We also performed [124] system demonstrations of real-time signal differentiations for Gaussian input pulses with a full-width at half maximum (FWHM) of ~ 0.12 ns, generated by an arbitrary waveform generator (AWG, KEYSIGHT M9505A). The waveform of the output signals after differentiation are shown in Figs. 6(a)–(d) (blue solid curves). They were recorded by means of a high-speed real-time oscilloscope (KEYSIGHT DSOZ504A Infiniium). For comparison, we also depict the ideal differentiation results, as shown in Figs. 6(a)–(d) (red dashed curves). The practical Gaussian pulse was used as the input RF signal for the simulation. One can see that the measured curves closely match their theoretical counterparts, indicating good agreement between experimental results and theory. Unlike the field differentiators, temporal derivatives of intensity profiles can be observed, indicating that intensity differentiation was successfully achieved. For the first-, second-, and third-order differentiators, the calculated RMSE between the measured and the theoretical curves are $\sim 4.15\%$, $\sim 6.38\%$, and $\sim 7.24\%$, respectively.

4. RF PHOTONIC TRUE TIME DELAY LINES (TTDLs)

In modern radar and communications systems, RF photonic true time delay lines (TTDLs), which introduce multiple progressive time delays by means of RF photonics technologies, are basic building blocks with wide applications in phased array antennas (PAAs), RF photonic filters, analog-to-digital or digital-to-analog conversion, and arbitrary waveform generation [110, 130, 131]. For RF photonic TTDLs, increasing the number of delay channels can lead to significantly improved performance. For instance, in PAAs, the number of radiating elements determines the beamwidth, and so an improved angular resolution can be achieved by increasing the channel number [132]. Consequently, RF photonic TTDLs with a large number of channels are highly desirable for PAAs with high angular resolution. In conventional methods, discrete lasers arrays [110, 133] or fiber Bragg grating (FBG) arrays [132] are employed for implementing multiple TTDL channels, and so system cost and complexity significantly increase with the rising channel number, thus greatly limiting the number of available channels in practical systems. In contrast, for a broadband Kerr optical micro-comb generated by a single micro-resonator, a large number of high-quality wavelength channels can be simultaneously provided for the RF photonic TTDL, thus greatly reducing the size, cost, and complexity of the system [134].

Figure 7(a) shows a schematic diagram of a multi-channel RF photonic TTDL with an optical micro-comb source. The TTDL is constructed with three modules. The first module generates the optical micro-comb with a large number of wavelength channels using a micro-resonator. The second module shapes the optical micro-comb and directs it to a Mach-Zehnder modulator (MZM), where replicas of the input RF signal are generated on each wavelength to establish multiple RF channels. Time delays were then introduced between the RF channels by dispersive elements in the third module. The measured time delay responses of a 21-channel RF photonic TTDL based on the optical micro-comb generated by a Hydex MRR with a FSR of ~ 200 GHz are shown in Fig. 7(b). We used two different lengths of dispersive single mode fibres (SMFs), yielding two different delay steps of ~ 118 ps/channel and ~ 59 ps/channel. As shown in Fig. 7(c), we also measured the time delay responses of an 81-channel RF photonic TTDL based on the optical micro-comb generated by another Hydex MRR with a FSR of ~ 49 GHz and got two delay steps of ~ 29.6 ps/channel and ~ 14.8 ps/channel for different lengths of the dispersive SMF. The time delay steps were jointly determined by the frequency spacing of the generated optical comb and the accumulated dispersion of the SMF, yielding the four different delay steps shown in Figs. 7(b) and (c). The optical spectra of the Kerr combs generated by the Hydex MRRs are shown in Figs. 7(d-i) and (d-ii) accordingly.

One of the important applications of an RF photonic TTDL is in phased array antenna (PAA) systems, where optical signals on selected channels are separately converted into the electrical domain and then fed to an antenna array to form radiating elements. Considering that the antenna array is a uniformly spaced linear array with an element spacing of d_{PAA} , the steering angle θ_0 of the PAA can be given as [111]

$$\theta_0 = \sin^{-1} \frac{c\tau}{d_{PAA}}, \quad (3)$$

where c is the speed of light in vacuum, and $\tau = mT$ ($m = 1, 2, 3, \dots$) is the time delay difference between adjacent radiating elements, with T denoting the time delay difference between adjacent delay channels. The steering angle can be tuned by adjusting τ , i.e., by changing the length of the dispersive medium or simply selecting every m_{th} channel as radiating elements. The corresponding array factor AF of the PAA can be expressed as [111]

$$AF(\theta, \lambda) = \frac{\sin^2 [M\pi(d_{PAA}/\lambda)(\sin\theta - c\tau/d_{PAA})]}{M^2 \sin^2 [\pi(d_{PAA}/\lambda)(\sin\theta - c\tau/d_{PAA})]} \quad (4)$$

where θ is the radiation angle, M is the number of radiating elements, and λ is the wavelength of the RF signals. The angular resolution of the PAA is the minimum angular separation at which two equal targets at the same range can be separated. It is determined by the 3-dB beamwidth of the PAA, which can be approximated as $\theta_{3dB} = 102 / M$ [112], thus indicating that the angular resolution would greatly increase with a larger number of radiating elements, and this can be realised via optical micro-combs that can provide numerous wavelength channels for beam steering.

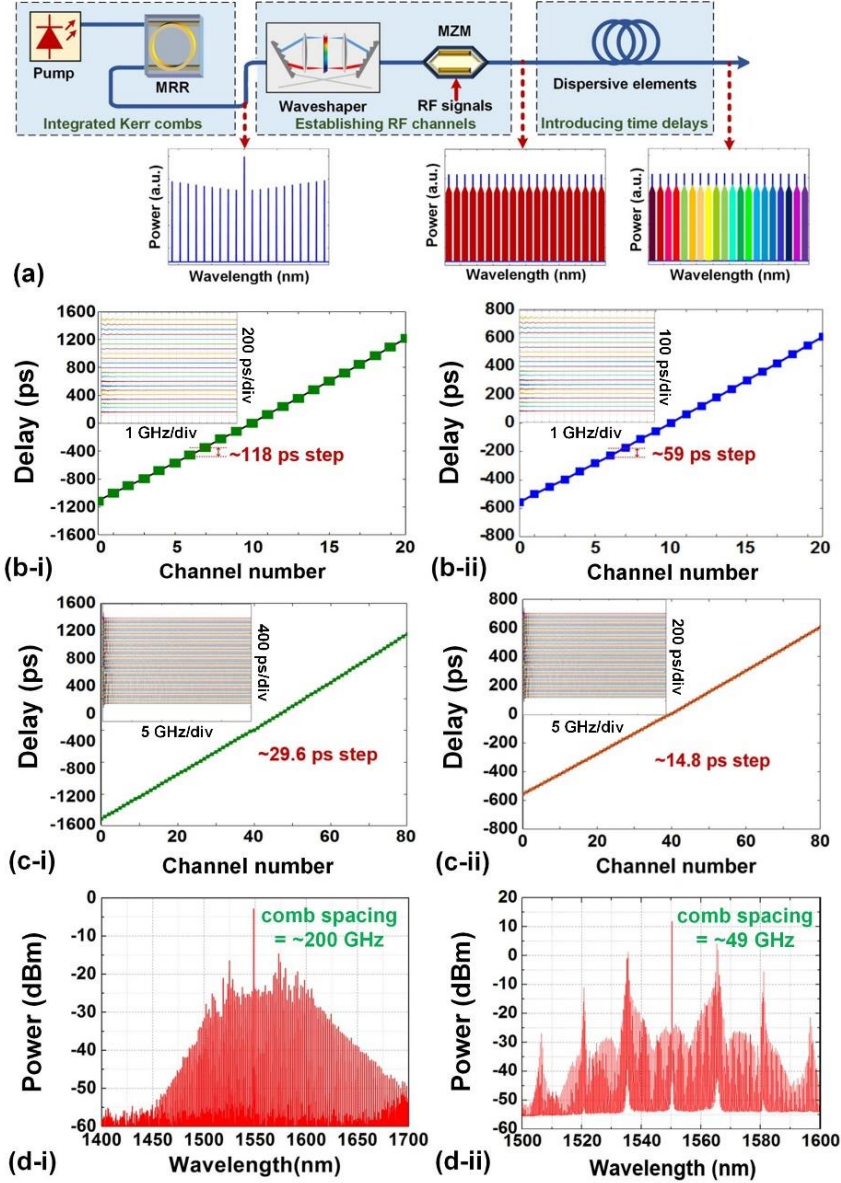


Fig. 7. RF photonic TTDs based on Hydex optical micro-comb sources. (a) Schematic diagram. MRR: micro-ring resonator. MZM: Mach-Zehnder modulator. (b) Measured time delay responses of a 21-channel TTDL with (i) 4-km-long dispersive SMF and (ii) 2-km-long dispersive SMF. (c) Measured time delay responses of an 81-channel TTDL with (i) 4-km-long dispersive SMF and (ii) 2-km-long dispersive SMF. Insets in (b) and (c) show the flat delays over a wide RF frequency range. (d) Optical spectra of the micro-combs generated by (i) the Hydex MRR with a FSR of ~ 200 GHz and (ii) the Hydex MRR with a FSR of ~ 49 GHz.

Figure 8(a) depicts the relationship between the number of radiating elements M and the 3-dB beamwidth θ_{3dB} of the PAA, where smaller beamwidths can be obtained when M increases, therefore suggesting, given the large number of available channels provided by the optical micro-comb based RF photonic TTDL, that the angular resolution for the PAA can be greatly enhanced. The improved angular resolution for increased M can also be observed in Fig. 8(b), which shows the AF of the PAA for different M calculated based on Eq. (4). To achieve a tunable beam steering angle, we selected every m_{th} ($m = 1, 2, 3, \dots$) wavelength of the TTDL by using the waveshaper, in such a way that the time delay (τ) between the radiating elements could be varied with a step size of T . Figures. 8(c) and (d) show the calculated AF for m ($m = \text{Channel number} / M$) varying from 1 to 7 based on a 200-GHz-FSR Hydex optical micro-comb and varying from 1 to 27 based on a 49-GHz-FSR Hydex optical micro-comb, respectively. As can be seen, the 49-GHz-FSR Kerr comb enables a much larger M as m varies, thus leading to a much smaller beamwidth and greatly enhanced angular resolution, as well as

finer tuning steps and a large tuning range of the beam steering angle because of the larger number of channels (m). Moreover, PAAs based on RF photonic TTDLs can also achieve wide instantaneous bandwidths without beam squint (the variation of beam steering angle as a function of RF frequency). As indicated in Figs. 8(e) and (f), the beam steering angle remains the same while the RF frequency varies. These results confirm that PAAs based on RF photonic TTDLs with an optical micro-comb source feature greatly improved angular resolution, a wide tunable range in terms of beam steering angle, and a large instantaneous bandwidth. By using tunable dispersive elements to replace the SMF, allowing a tunable adjustment in time delay [136], optical micro-comb based two-dimensional PAAs with continuously-tunable time delays can be further realised.

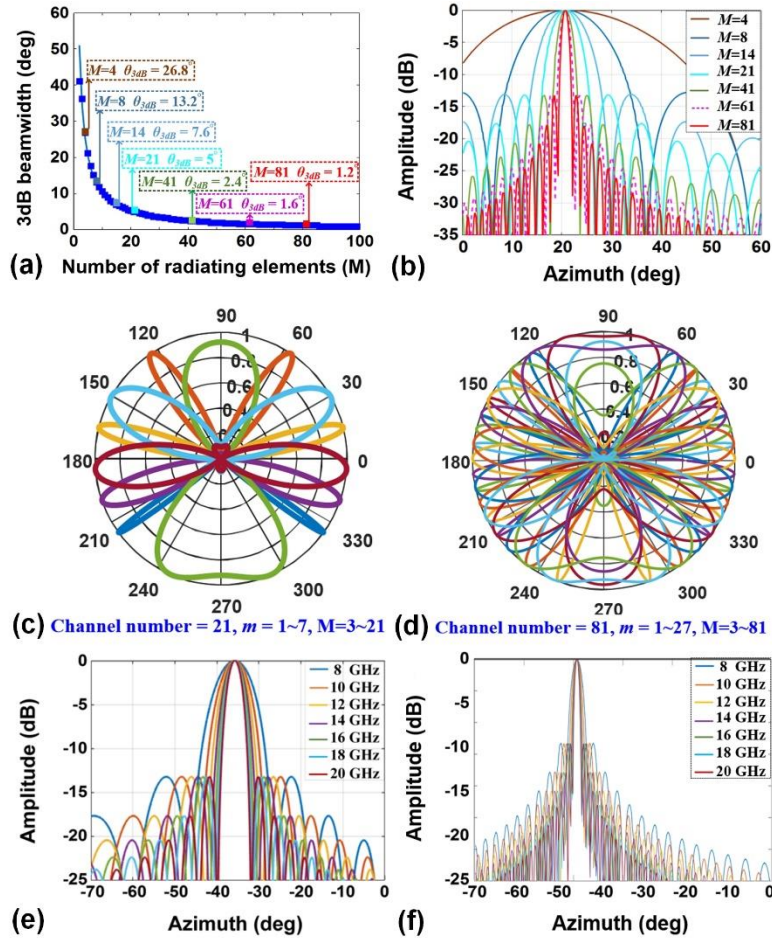


Fig. 8. (a) Relationship between the number of radiating elements M and the 3dB beamwidth θ_{3dB} of the PAA. (b) Calculated AF of the PAA with M varying from 4 to 81 based on a 49-GHz-FSR Hydex optical micro-comb. (c) Calculated AF of the PAA with m varying from 1 to 7 based on a 200-GHz-FSR Hydex optical micro-comb. (d) Calculated AF of the PAA with m varying from 1 to 27 based on a 49-GHz-FSR Hydex micro-comb. (e) Calculated AF of the PAA with various RF frequencies based on a 200-GHz-FSR Hydex optical micro-comb. (f) Calculated AF of the PAA with various RF frequencies based on a 49-GHz-FSR Hydex optical micro-comb.

5. CONCLUSION

Optical micro-combs represent an exceptionally active field of research that has only developed in the last ten years. This young and fast-growing field has its roots in the pioneering development of high-Q micro-cavity technologies, starting in the late 1980s and experiencing significant recent advances, both for bulk and integrated resonators. We review our recent progress in using optical micro-combs in the context of RF and microwave photonic signal processing. We demonstrate a reconfigurable microwave photonic intensity differentiator based on an integrated Kerr comb source. The Kerr optical comb is produced via a CMOS-compatible nonlinear MRR, which greatly increases the processing bandwidth and has the

potential for a low cost, size, and complexity processing system. By programming and shaping the individual comb lines' power according to the calculated tap weights, we successfully demonstrate the first-, second-, and third-order intensity differentiations of the RF signal. The RF amplitude and phase responses of the proposed differentiator are characterized, and system demonstrations of real-time differentiations are performed for Gaussian input pulses. We achieve good agreement between theory and experimental results, thus verifying the effectiveness of our method. We also demonstrate optical true time delays for advanced RF radar applications. Our approach of using microcombs for RF and microwave signal processing provides a new way to implement microwave photonic signal processing functions with compact device footprint, high processing bandwidth, and high reconfigurability, thus holding great promise for future ultra-high-speed computing and information processing.

6. ACKNOWLEDGMENTS

This work was supported by the Australian Research Council Discovery Projects Program (No. DP150104327). RM acknowledges support by Natural Sciences and Engineering Research Council of Canada (NSERC) through the Strategic, Discovery and Acceleration Grants Schemes, by the MESI PSR-SIIRI Initiative in Quebec, and by the Canada Research Chair Program. He also acknowledges additional support by the Government of the Russian Federation through the ITMO Fellowship and Professorship Program (grant 074-U 01) by the 1000 Talents Sichuan Program. BEL was supported by the Strategic Priority Research Program of the Chinese Academy of Sciences, Grant No. XDB24030000.

References

- [1] B.J. Eggleton, S.Radic, and D.J. Moss, Chapter 20, p759-828 in *Optical Fiber Telecommunications V: Components and Sub-systems*, Edited by Ivan P. Kaminow, Tingye Li, and Alan E. Willner, Academic Press, Oxford, UK, February (2008).
- [2] J. Leuthold, C. Koos, and W. Freude, *Nat. Photon.* **4** (8), 535 (2010).
- [3] Li, F. et al., *Optics Express* **19**, 20364-20371 (2011). DOI: 10.1364/OE.19.020364.
- [4] Li, F. et al., *Optics Express* **18**, 3905-3910 (2010). DOI: 10.1364/OE.18.003905.
- [5] H.Ji, *et.al.*, *Photonics Technology Letters* **22** 1762 (2010).
- [6] Monat, C. et al., *Optics Express* **18** (7), 6831-6840 (2010). DOI: 10.1364/OE.18.006831.
- [7] Corcoran, B., et. al., *Optics Express* **18**, (8) 7770-7781 (2010). DOI: 10.1364/OE.18.007770.
- [8] V.G. Ta'eed, et al., *Optics Letters* **30** 2900 (2005). DOI: 10.1364/OL.30.002900.
- [9] M. Rochette, J. Kutz, J. Blows, D. Moss, J. T. Mok, and B. J. Eggleton, *IEEE Photonics Technology Letters* **17** 908 (2005).
- [10] M.Ferrera et al., *Optics Express* **22** (18) 21488 - 21498 (2014). DOI: 10.1364/OE.22.021488.
- [11] C.Monat et al., *Nature Communications* **5** Article:3246 (2014). doi:10.1038/ncomms4246.
- [12] F. Li, et al., *Optics Express* **19**, (23) 22410-22416 (2011).
- [13] T.D. Vo, et al., *IEEE Journal of Lightwave Technology* **29** (12) 1790-1796 (2011).
- [14] M.Ferrera, et al., *Optics Express* **19** (23) 23153-23161 (2011).
- [15] B. Corcoran, et al., *Optics Express* **18** 20190 (2010). DOI: 10.1364/OE.18.020190.
- [16] L.Caspani, et al., *J. of the Optical Society of America B, JOSA B* **28** (12) A67-A82 (2011). DOI:10.1364/JOSAB.28.000A67
- [17] B.Corcoran, et al., *Nature Photonics* **3** (4) 206 (2009). doi:10.1038/nphoton.2009.28.
- [18] D. J. Moss, H. M. van Driel, and J. E. Sipe, *Opt. Lett.* **14** (1), 57 (1989).
- [19] J. E. Sipe, D. J. Moss, and H. M. van Driel, *Phys. Rev. B* **35** (3), 1129 (1987).
- [20] D. J. Moss, E. Ghahramani, J. E. Sipe, and H. M. van Driel, *Phys. Rev. B* **41** (3), 1542 (1990).
- [21] D. J. Moss, H. M. van Driel, and J. E. Sipe, *Appl. Phys. Lett.* **48** (17) 1150 (1986).
- [22] D.J.Moss, et al., *Electronics Letters* **41** 320 (2005). DOI:10.1049/el:20058051
- [23] M.R.E. Lamont, et al., *Photonics Technology Letters* **18** 1185 (2006). DOI:10.1109/LPT.2006.874718.
- [24] A.Tuniz, G.Brawley, D.J.Moss, B.J.Eggleton,, *Optics Express* **16** 18524 (2008). DOI: 10.1364/OE.16.018524.
- [25] B.J Eggleton, B Luther-Davies, K Richardson, "Chalcogenide photonics", *Nature Photonics* **5** (3), 141 (2011).
- [26] M.Lee, et al., *Optics Express* **15** 1277-1285 (2007). DOI:10.1364/OE.15.001277
- [27] S. Tomljenovic-Hanic, M.J. Steel, C. Martijn de Sterke and D. J. Moss, "High-Q cavities in photosensitive photonic crystals", *Optics Letters* **32** (5) 542-544 (2007). DOI:10.1364/OL.32.000542
- [28] C.Grillet, et al., *Optics Express* **15** (3) 1267-1276 (2007). DOI:10.1364/OE.15.001267
- [29] V.G. Ta'eed, N. Baker, L. Fu, K. Finsterbusch, M.R.E. Lamont, H.Nguyen, D.J. Moss, and B.J. Eggleton, Y. Choi, S. Madden, B. Luther-Davies "Ultrafast all-optical chalcogenide glass photonic circuits", *Optics Express* **15** 9205 (2007).

- [30] D. Freeman, C. Grillet, M. Lee, B. Luther-Davies, CLC Smith, Y. Ruan, A. Rode, D. J. Moss, and B. J. Eggleton, "Chalcogenide Glass Photonic Crystal Devices", *Photonic and Electromagnetic Crystal Structures, Photonics and Nanostructures-Fundamentals and Applications*, Science Direct Elsevier Publishing **6** (1) Pages: 3-11 (2008). doi:10.1016/j.photonics.2007.11.001.
- [31] C. Grillet, D. Freeman, B. Luther-Davies, S. Madden, R. McPhedran, D. J. Moss, M. J. Steel, and B. J. Eggleton, "Characterization and modeling of Fano resonances in chalcogenide photonic crystal membranes", *Optics Express* **14** 369 (2006).
- [32] V. G. Ta'eed, M. Shokooh-Saremi, L. B. Fu, D. J. Moss, M. Rochette, I. C. M. Littler, B. J. Eggleton, Y. Ruan and B. Luther-Davies, "Self-phase modulation based integrated optical regeneration in chalcogenide waveguides", *IEEE Journal of Selected Topics in Quantum Electronics* **12** 360 (2006).
- [33] M. Shokooh-Saremi, V. G. Ta'eed, I. Littler, D. J. Moss and B. J. Eggleton, Y. Ruan and B. Luther-Davies, "High performance Bragg gratings in chalcogenide rib waveguides written with a modified Sagnac interferometer: experiment and modeling", *Journal of the Optical Society of America B (JOSA B)* **23** 1323 (2006).
- [34] M. R. E. Lamont, V. G. Ta'eed, M. A. F. Roelens, D. J. Moss, B. J. Eggleton, D. Y. Choy, S. Madden and B. Luther-Davies, "Error-free wavelength conversion via cross phase modulation in 5 cm of As₂S₃ chalcogenide glass rib waveguide", *Electronics Letters* **43** 945 (2007).
- [35] Ikeda, K., Saperstein, R. E., Alic, N. & Fainman, Y., "Thermal and Kerr nonlinear properties of plasma-deposited silicon nitride/silicon dioxide waveguides", *Opt. Express* **16**, 12987–12994 (2008).
- [36] J. S. Levy, A. Gondarenko, M. A. Foster *et al.*, "CMOS-compatible multiple-wavelength oscillator for on-chip optical interconnects," *Nature Photonics* **4** (1), 37-40 (2010).
- [37] L. Razzari, D. Duchesne, M. Ferrera *et al.*, "CMOS-compatible integrated optical hyper-parametric oscillator," *Nature Photonics* **4** (1), 41-45 (2010).
- [38] D. J. Moss, R. Morandotti, A. L. Gaeta *et al.*, "New CMOS-compatible platforms based on silicon nitride and Hydex for nonlinear optics," *Nature Photonics* **7** (8), 597-607 (2013).
- [39] M. Ferrera, L. Razzari, D. Duchesne *et al.*, "Low-power continuous-wave nonlinear optics in doped silica glass integrated waveguide structures," *Nature Photonics*, **2** (12), 737-740 (2008).
- [40] M. Ferrera, D. Duchesne, L. Razzari *et al.*, "Low power four wave mixing in an integrated, micro-ring resonator with Q=1.2 million," *Optics Express*, **17** (16), 14098-14103 (2009).
- [41] D. Duchesne, M. Peccianti, M. R. E. Lamont *et al.*, "Supercontinuum generation in a high index doped silica glass spiral waveguide," *Optics Express*, **18** (2), 923-930 (2010).
- [42] M. Ferrera, *et al.*, "On-chip CMOS-compatible all-optical integrator", *Nature Communications*, **1** Article 29 (2010). DOI:10.1038/ncomms1028
- [43] A. Pasquazi, R. Ahmad, M. Rochette *et al.*, "All-optical wavelength conversion in an integrated ring resonator," *Optics Express*, **18** (4), 3858-3863 (2010).
- [44] A. Pasquazi, Y. Park, J. Azana *et al.*, "Efficient wavelength conversion and net parametric gain via Four Wave Mixing in a high index doped silica waveguide," *Optics Express*, **18** (8), 7634-7641 (2010).
- [45] M. Peccianti, M. Ferrera, L. Razzari *et al.*, "Subpicosecond optical pulse compression via an integrated nonlinear chirper," *Optics Express*, **18** (8), 7625-7633 (2010).
- [46] D. Duchesne, M. Ferrera, L. Razzari *et al.*, "Efficient self-phase modulation in low loss, high index doped silica glass integrated waveguides," *Optics Express*, **17** (3), 1865-1870 (2009).
- [47] Pasquazi, M. Peccianti, L. Razzari, D. J. Moss, S. Coen, M. Erkintalo, Y. K. Chembo, T. Hansson, S. Wabnitz, P. Del'Haye, X. Xue, A. M. Weiner, and R. Morandotti, *Physics Reports* **729** (1), 1 (2018).
- [48] P. Del'Haye, A. Schliesser, O. Arcizet, T. Wilken, R. Holzwarth, T. J. Kippenberg, "Optical frequency comb generation from a monolithic microresonator", *Nature* **450** 1214–1217 (2007).
- [49] M. Peccianti, A. Pasquazi, Y. Park, B. E. Little, S. Chu, D. J. Moss, and R. Morandotti, "Demonstration of an ultrafast nonlinear microcavity modelocked laser", *Nature Communications*, **3** 765 (2012). DOI:10.1038/ncomms1762
- [50] M. Kues, *et al.*, "Passively modelocked laser with an ultra-narrow spectral width", *Nature Photonics*, **11** (3) 159 (2017). DOI:10.1038/nphoton.2016.271
- [51] A. Pasquazi, L. Caspani, M. Peccianti *et al.*, "Self-locked optical parametric oscillation in a CMOS compatible microring resonator: a route to robust optical frequency comb generation on a chip," *Optics Express*, **21** (11), 13333-13341 (2013).
- [52] A. Pasquazi, M. Peccianti, B. E. Little *et al.*, "Stable, dual mode, high repetition rate mode-locked laser based on a microring resonator," *Optics Express*, **20** (24), 27355-27362 (2012).

- [53] C. Reimer, L. Caspani, M. Clerici *et al.*, “Integrated frequency comb source of heralded single photons,” *Optics Express*, **22** (6), 6535-6546 (2014).
- [54] C.Reimer, et al., “Cross-polarized photon-pair generation and bi-chromatically pumped optical parametric oscillation on a chip”, *Nature Communications*, **6** Article 8236 (2015). DOI: 10.1038/ncomms9236
- [55] L. Caspani, C. Reimer, M. Kues *et al.*, “Multifrequency sources of quantum correlated photon pairs on-chip: a path toward integrated Quantum Frequency Combs,” *Nanophotonics*, **5** (2), 351-362 (2016).
- [56] C. Reimer, M. Kues, P. Roztocki *et al.*, “Generation of multiphoton entangled quantum states by means of integrated frequency combs,” *Science*, **351** (6278), 1176-1180 (2016).
- [57] M.Kues, et al., “On-chip generation of high-dimensional entangled quantum states and their coherent control”, *Nature*, **546** (7660) 622-626 (2017).
- [58] P. Roztocki, M. Kues, C. Reimer *et al.*, “Practical system for the generation of pulsed quantum frequency combs,” *Optics Express*, **25** (16), 18940-18949 (2017).
- [59] P.Marin-Palomo, et al., “Microresonator-based solitons for massively parallel coherent optical communications”, *Nature* **546** (7657) 274 (2017).
- [60] DT Spencer et al., “An optical-frequency synthesizer using integrated photonics”, *Nature* **557** (7703) 81-85 (2018).
- [61] J Pfeifle, V Brasch, M Lauermaun, Y Yu, D Wegner, T Herr, K Hartinger, et al., “Coherent terabit communications with microresonator Kerr frequency combs”, *Nature Photonics* **8** (5), 375-380 (2014).
- [62] P Del’Haye, T Herr, E Gavartin, ML Gorodetsky, R Holzwarth, et al., “Octave spanning tunable frequency comb from a microresonator”, *Physical Review Letters* **107** (6), 063901 (2011).
- [63] TJ Kippenberg, R Holzwarth, SA Diddams, “Microresonator-based optical frequency combs”, *Science* **332** (6029), 555-559 (2011).
- [64] T Herr, V Brasch, JD Jost, CY Wang, NM Kondratiev, ML Gorodetsky, et al., “Temporal solitons in optical microresonators”, *Nature Photonics* **8** (2), 145-152 (2014).
- [65] F Ferdous, H Miao, DE Leaird, K Srinivasan, J Wang, L Chen, ... “Spectral line-by-line pulse shaping of on-chip microresonator frequency combs”, *Nature Photonics* **5** (12), 770 (2011).
- [66] X Xue, PH Wang, Y Xuan, M Qi, AM Weiner, “Microresonator Kerr frequency combs with high conversion efficiency”, *Laser & Photonics Reviews* **11** (1) (2017).
- [67]Y Xuan, Y Liu, LT Varghese, AJ Metcalf, X Xue, PH Wang, K Han, ... “High-Q silicon nitride microresonators exhibiting low-power frequency comb initiation”, *Optica* **3** (11), 1171-1180 (2016).
- [68] X Xue, M Qi, AM Weiner, “Normal-dispersion microresonator Kerr frequency combs”, *Nanophotonics* **5** (2), 244-262 (2016).
- [69] C.Grillet, et al., “Amorphous Silicon Nanowires with Record High Nonlinearity, FOM, and Optical Stability”, *Optics Express* **20** (20) 22609-22615 (2012). DOI: 10.1364/OE.20.022609.
- [70] J. Capmany, and D. Novak, “Microwave photonics combines two worlds,” *Nature Photonics*, **1**(6), 319-330 (2007).
- [71] J. Capmany, J. Mora, I. Gasulla, J. Sancho, J. Lloret, and S. Sales, “Microwave Photonic Signal Processing,” *Journal of Lightwave Technology*, **31**, (4) pp. 571-586 (2013).
- [72] A. J. Seeds, “Microwave photonics,” *IEEE Transactions on Microwave Theory and Techniques*, **50** (3), 877-887 (2002).
- [73] R. C. Williamson, and R. D. Esman, “RF photonics,” *Journal of Lightwave Technology*, **26** (9-12), 1145-1153 (2008).
- [74] J. P. Yao, “Microwave Photonics,” *IEEE Journal of Lightwave Technology*, **27** (1-4), 314-335 (2009).
- [75] V. R. Supradeepa, C.M. Long, R.Wu, F.Ferdous, E.Hamidi, D.E. Leaird, and A.M. Weiner, “Comb-based radiofrequency photonic filters with rapid tunability and high selectivity,” *Nature Photonics* **6**, 186–194 (2012).
- [76] V. R. Supradeepa, C. M. Long, R. Wu, F. Ferdous, E. Hamidi, D. E. Leaird, and A. M. Weiner, “Comb-based radiofrequency photonic filters with rapid tunability and high selectivity,” *Nature Photonics*, **6**, (3) 186-194 (2012).
- [77] MH Khan, H Shen, Y Xuan, L Zhao, S Xiao, DE Leaird, AM Weiner, M Qi, “Ultrabroad-bandwidth arbitrary radiofrequency waveform generation with a silicon photonic chip-based spectral shaper”, *Nature Photonics* **4** (2), 117 (2010).
- [78] A Fülöp, M Mazur, A Lorences-Riesgo, TA Eriksson, PH Wang, Y Xuan, ... “Long-haul coherent communications using microresonator-based frequency combs”, *Optics Express* **25** (22), 26678-26688 (2017).
- [79] V. Torres-Company and A.M. Weiner, “Optical frequency comb technology for ultra-broadband radio-frequency photonics,” *Laser & Photonics Reviews* **8** (3) 368-393 (2014).
- [80] D. Marpaung, M. Pagani, B. Morrison *et al.*, “Nonlinear Integrated Microwave Photonics,” *IEEE Journal of Lightwave Technology*, **32** (20), 3421-3427 (2014).

- [81] Q. Z. Cen, Y. T. Dai, F. F. Yin *et al.*, "Rapidly and continuously frequency-scanning opto-electronic oscillator," *Optics Express*, **25** (2), 635-643 (2017).
- [82] J. Dai, X. Y. Xu, J. L. Ke *et al.*, "Self-Oscillating Triangular Pulse Generator Based on 90 degrees Photonic-Assisted Phase Shifter," *IEEE Photonics Technology Letters*, **29** (3), 271-274 (2017).
- [83] J. Dai, X. Y. Xu, Z. L. Wu *et al.*, "Self-oscillating optical frequency comb generator based on an optoelectronic oscillator employing cascaded modulators," *Optics Express*, **23** (23), 30014-30019 (2015).
- [84] K. Xu, R. X. Wang, Y. T. Dai *et al.*, "Microwave photonics: radio-over-fiber links, systems, and applications," *Photonics Research*, **2** (4), B54-B63 (2014).
- [85] X. Y. Xu, J. Dai, Y. T. Dai *et al.*, "Broadband and wide-range feedback tuning scheme for phase-locked loop stabilization of tunable optoelectronic oscillators," *Optics Letters*, **40** (24), 5858-5861 (2015).
- [86] A. X. Zhang, Y. T. Dai, F. F. Yin *et al.*, "Stable radio-frequency delivery by lambda dispersion-induced optical tunable delay," *Optics Letters*, **38** (14), 2419-2421 (2013).
- [87] S. Mansoori, and A. Mitchell, "RF transversal filter using an AOTF," *IEEE Photonics Technology Letters*, **16** (3), 879-881 (2004).
- [88] H. Emami, N. Sarkhosh, L. A. Bui *et al.*, "Wideband RF photonic in-phase and quadrature-phase generation," *Optics Letters*, **33** (2), 98-100 (2008).
- [89] S. L. Pan, and J. P. Yao, "Optical generation of polarity- and shape-switchable ultrawideband pulses using a chirped intensity modulator and a first-order asymmetric Mach-Zehnder interferometer," *Optics Letters*, **34** (9), 1312-1314 (2009).
- [90] D. Marpaung, C. Roeloffzen, R. Heideman *et al.*, "Integrated microwave photonics," *Laser & Photonics Reviews*, **7** (4), 506-538 (2013).
- [91] E. Hamidi, D. E. Leaird, and A. M. Weiner, "Tunable Programmable Microwave Photonic Filters Based on an Optical Frequency Comb," *IEEE Transactions on Microwave Theory and Techniques*, **58** (11), 3269-3278 (2010).
- [92] J. Y. Wu, P. Cao, X. F. Hu *et al.*, "Compact tunable silicon photonic differential-equation solver for general linear time-invariant systems," *Optics Express*, **22** (21), 26254-26264 (2014).
- [93] J. Y. Wu, P. Cao, X. F. Hu *et al.*, "Nested Configuration of Silicon Microring Resonator With Multiple Coupling Regimes," *IEEE Photonics Technology Letters*, **25** (6), 580-583 (2013).
- [94] J. Y. Wu, P. Cao, T. Pan *et al.*, "Compact on-chip 1 x 2 wavelength selective switch based on silicon microring resonator with nested pairs of subrings," *Photonics Research*, **3** (1), 9-14 (2015).
- [95] J. Y. Wu, B. Y. Liu, J. Z. Peng *et al.*, "On-Chip Tunable Second-Order Differential-Equation Solver Based on a Silicon Photonic Mode-Split Microresonator," *IEEE Journal of Lightwave Technology*, **33** (17), 3542-3549 (2015).
- [96] J. Y. Wu, J. Z. Peng, B. Y. Liu *et al.*, "Passive silicon photonic devices for microwave photonic signal processing," *Optics Communications*, **373**, 44-52 (2016).
- [97] J. Wu, T. Moein, X. Xu, G. Ren, A. Mitchell, and D. J. Moss, "Micro-ring resonator quality factor enhancement via an integrated Fabry-Perot cavity," *Applied Physics Letters (APL) Photonics*, **2**, 056103 (2017).
- [98] O. F. Yilmaz, L. Yaron, S. Khaleghi *et al.*, "True time delays using conversion/dispersion with flat magnitude response for wideband analog RF signals," *Optics Express*, **20** (8), 8219-8227 (2012).
- [99] R. Wu, V. Torres-Company, D. E. Leaird *et al.*, "Supercontinuum-based 10-GHz flat-topped optical frequency comb generation," *Optics Express*, **21** (5), 6045-6052 (2013).
- [100] A. J. Metcalf, V. Torres-Company, D. E. Leaird *et al.*, "High-Power Broadly Tunable Electrooptic Frequency Comb Generator," *IEEE Journal of Selected Topics in Quantum Electronics*, **19** (6), (2013).
- [101] Y. C. Han, Z. Li, and J. P. Yao, "A Microwave Bandpass Differentiator Implemented Based on a Nonuniformly-Spaced Photonic Microwave Delay-Line Filter," *IEEE Journal of Lightwave Technology*, **29** (22), 3470-3475 (2011).
- [102] J. Azana, C. Madsen, K. Takiguchi *et al.*, "Guest editorial - Optical signal processing," *IEEE Journal of Lightwave Technology*, **24** (7), 2484-2486 (2006).
- [103] R. Slavik, Y. Park, M. Kulishov *et al.*, "Ultrafast all-optical differentiators," *Optics Express*, **14** (22), 10699-10707 (2006).
- [104] J. Azana, "Ultrafast Analog All-Optical Signal Processors Based on Fiber-Grating Devices," *IEEE Photonics Journal*, **2** (3), 359-386 (2010).
- [105] R. Ashrafi, M. H. Asghari, and J. Azana, "Ultrafast Optical Arbitrary-Order Differentiators Based on Apodized Long-Period Gratings," *IEEE Photonics Journal*, **3** (3), 353-364 (2011).
- [106] R. Ashrafi, and J. Azana, "Figure of merit for photonic differentiators," *Optics Express*, **20** (3), 2626-2639 (2012).

- [107] J. McClellan, T. Parks, and L. Rabiner, "A computer program for designing optimum FIR linear phase digital filters," *IEEE Transactions on Audio and Electroacoustics*, **21** (6), 506-526 (1973).
- [108] T. Herr, K. Hartinger, J. Riemensberger *et al.*, "Universal formation dynamics and noise of Kerr-frequency combs in microresonators," *Nature Photonics*, **6** (7), 480-487 (2012).
- [109] L.Di Lauro, J.Li, D.J. Moss, R.Morandotti, S.T. Chu, M.Peccianti, A.Pasquazi, "Parametric Control of Thermal Self-Pulsation in Microcavity", *Optics Letters* **42** (17) 3407 – 3410 (2017).
- [110] J. J. Zhang, and J. P. Yao, "Photonic True-Time Delay Beamforming Using a Switch-Controlled Wavelength-Dependent Recirculating Loop," *Journal of Lightwave Technology*, **34** (16), 3923-3929 (2016).
- [111] M. Longbrake, "True Time-Delay Beamsteering for Radar," *Proceedings of the 2012 IEEE National Aerospace and Electronics Conference (Naecon)*, pp. 246-249, 2012.
- [112] M. I. Skolnik, "Introduction to radar systems," 3rd ed. New York, NY: McGraw-Hill, 2001.
- [113] J. Capmany, B. Ortega, and D. Pastor, "A tutorial on microwave photonic filters," *Journal of Lightwave Technology*, **24**, (1) 201-229 (2006).
- [114] J. Capmany, B. Ortega, D. Pastor, and S. Sales, "Discrete-time optical processing of microwave signals," *Journal of Lightwave Technology*, **23** (2) 702-723 (2005).
- [115] A. Ortigosa-Blanch, J. Mora, J. Capmany, B. Ortega, and D. Pastor, "Tunable radio-frequency photonic filter based on an actively mode-locked fiber laser," *Optics Letters*, **31**, (6) 709-711 (2006).
- [116] W. L. Liu, M. Li, R. S. Guzzon, E. J. Norberg, J. S. Parker, M. Z. Lu, L. A. Coldren, and J. P. Yao, "A fully reconfigurable photonic integrated signal processor," *Nature Photonics*, **10** (3) 190 (2016).
- [117] HJ Kim, DE Leaird, AM Weiner, "Rapidly tunable dual-comb RF photonic filter for ultrabroadband RF spread spectrum applications", *IEEE Transactions on Microwave Theory and Techniques* **64** (10), 3351-3362 (2016).
- [118] J. Wu, X. Xu, R., and D. J. Moss, "RF photonics: An optical micro-combs' perspective", *IEEE Journal of Selected Topics in Quantum Electronics* **24** (4) 1-20 (2018). DOI: 10.1109/JSTQE.2018.2805814.
- [119] X. X. Xue, Y. Xuan, H. J. Kim, J. Wang, D. E. Leaird, M. H. Qi, and A. M. Weiner, "Programmable Single-Bandpass Photonic RF Filter Based on Kerr Comb from a Microring," *IEEE Journal of Lightwave Technology*, **32** (20) 3557-3565 (2014).
- [120] X.X.Xue and A.M. Weiner, "Microwave photonics connected with microresonator frequency combs", *Frontiers of Optoelectronics* **9** (2) 238-248 (2016).
- [121] X Xue, Y Xuan, C Bao, S Li, X Zheng, B Zhou, M Qi, AM Weiner, "Microcomb-based true-time-delay network for microwave beamforming with arbitrary beam pattern control", *Journal of Lightwave Technology* **36** (12), 2312-2321 (2018).
- [122] X.Xu, J.Wu, M.Shoeiby, T.G. Nguyen, S.T. Chu, B.E. Little, R. Morandotti, A.Mitchell, and D.J. Moss, "Advanced RF and microwave functions based on an integrated optical frequency comb source", *Optics Express* **26** (3), 2569-2583 (2018).
- [123] T. G. Nguyen, M. Shoeiby, S. T. Chu *et al.*, "Integrated frequency comb source based Hilbert transformer for wideband microwave photonic phase analysis," *Optics Express*, **23** (17), 22087-22097 (2015).
- [124] X.Xu, *et al.*, "Reconfigurable broadband microwave photonic intensity differentiator based on an integrated optical frequency comb source", *Applied Physics Letters (APL) Photonics*, **2** (9) 096104 (2017). DOI: 10.1063/1.4989871.
- [125] X. X. Xue, Y. Xuan, H. J. Kim *et al.*, "Programmable Single-Bandpass Photonic RF Filter Based on a Kerr Comb from a Microring," *IEEE Journal of Lightwave Technology*, **32** (20), 3557-3565 (2014).
- [126] X.Xu, J.Wu, T.G. Nguyen, S.T. Chu, B.E. Little, R.Morandotti, A.Mitchell, and D. J. Moss, "Continuously tunable orthogonally polarized optical RF single sideband generator and equalizer based on an integrated micro-ring resonator", submitted, *IEEE Journal of Lightwave Technology (JLT)* **36** (12) p (2018).
- [127] X. Y. Xu, J. Y. Wu, T. G. Nguyen, S. T. Chu, B. E. Little, R. Morandotti, A. Mitchell, and D. J. Moss, "Integrated optical power equalizer based on a dual-polarization micro-ring resonator," in *CLEO: QELS_Fundamental Science*, San Jose, CA, May 2018, Paper JW2A.22.
- [128] X.Xu, J.Wu, T.G. Nguyen, S.T. Chu, B.E. Little, R.Morandotti, A.Mitchell, and D.J. Moss, "Broadband RF Channelizer based on an Integrated Optical Frequency Comb Source", *IEEE Journal of Lightwave Technology (JLT) Special Issue on Microwave Photonics* **36** (12) p (2018). DOI: 10.1109/JLT.2018.2819172
- [129] X.Xu, J.Wu, T.G. Nguyen, T.Moein, S.T. Chu, B. E. Little, R.Morandotti, A.Mitchell, and D.J. Moss, "Photonic microwave true time delays for phased array antennas using a 49GHz FSR integrated optical micro-comb source", *OSA Photonics Research Journal, Special Issue on Integrated Nonlinear Photonics* **6** (5) B30-B36 (2018). DOI:10.1364/PRJ.6.000B30

- [130] D. H. Yang and W. P. Lin, "Phased-array beam steering using optical true time delay technique," *Opt. Commun.*, **350** 90–96 (2015).
- [131] X. W. Ye, F. Z. Zhang, and S. L. Pan, "Optical true time delay unit for multi-beamforming," *Opt. Express*, **23**, (8) 10002–10008 (2015).
- [132] Y. Q. Liu, J. P. Yao, and J. L. Yang, "Wideband true-time-delay unit for phased array beamforming using discrete-chirped fiber grating prism," *Opt. Commun.*, **207**, (1–6) 177–187, (2002).
- [133] S. Chin et al., "Broadband true time delay for microwave signal processing, using slow light based on stimulated Brillouin scattering in optical fibers," *Opt. Express*, **18**, (21) 22599–22613 (2010).
- [134] X. Xue et al., "Microcomb-based microwave photonics," in *Proc. Asia Commun. Photon. Conf.*, Guangzhou, China, 2017, Paper Su3E.2.
- [135] M. Longbrake, "True time-delay beamsteering for radar," in *Proc. 2012 IEEE Nat. Aerosp. Electron. Conf.*, 2012, pp. 246–249.
- [136] X. W. Ye, F. Z. Zhang, and S. L. Pan, "Compact optical true time delay beamformer for a 2D phased array antenna using tunable dispersive elements," *Opt. Lett.*, **41**, (17) 3956–3959 (2016).